ASSESSING WOUND ROLL QUALITY USING A MEASURED STIFFNESS/MODEL METHOD

By

R. Markum and J. K. Good
Oklahoma State University
USA

ABSTRACT

For those concerned with roll quality it is difficult to suppress the urge to compress the outer surface of a wound roll with your thumb to sense how tightly the roll was wound and how large the internal pressures might be. If several rolls of a given web are wound at unique tensions a human could often arrange these rolls in order of ascending winding tension using the~~ir~~ thumb test. The thumb senses the relative conforming deformation of the roll surface. A soft roll would deform more and have greater contact area with our thumb than a hard roll for a given load. The thumb test is most useful on softer rolls wound from nonwovens, tissues, some grades of paper and polymer films but less so on metal coils that deform little in comparison to our thumb. The physics define *stiffness* as the extent to which an object resists deformation in response to an applied force. This publication reports the results of research where the stiffness of the outer surface of a wound roll is used to characterize the internal residual stresses throughout the roll due to winding. Measurements of stiffness of the outer surface of wound rolls will be demonstrated using commercially available devices along with a proposed handheld device all having greater resolution than the thumb. These measurements will be coupled with models to allow the exploration of internal residual stresses in the wound roll that can be used to investigate winding defects and roll quality.

INTRODUCTION

Wound roll quality can be an ambiguous term based on the perspectives of those concerned. For those who wound the roll, good quality might mean the roll was successfully wound with no mishaps that resulted in lateral offsets or splices and has sufficient structure to be transported to the next process. If hardness was assessed at this point and deviations were found across the roll width this could be a perspective of poor quality and point to upstream process problems, non-uniformity in web formation, or coating for example. Those unwinding the roll might agree that offsets and splices are

undesirable, but might also claim poor roll quality due to telescoping, buckles, bagginess and blocking, viscoelastic changes, and other defects, that were unapparent when the roll was wound, resulted in productivity loss in their converting process. Perhaps the ultimate roll quality is achieved when all perspectives are satisfied and the roll is wound and unwound with no waste. Techniques for monitoring roll quality should provide means that allow all perspectives to be satisfied.

Humans make hundreds or perhaps thousands assessments of stiffness each day of our lives. How hard do you press a key on a keyboard before you elect to release it [1]? Would you elect not to purchase a soft apple but possibly a peach that yields slightly to your touch [2]? Even though humans are capable of some assessment of the stiffness of wound rolls it has never been documented, perhaps due to the assessment being too qualitative or inapplicable to hard rolls of high stiffness.

There have been several devices used that are intended to measure roll hardness in some form. The earliest devices were wooden clubs which when struck across the width of the wound roll to qualitatively seek out regions where the web thickness and as a result the pressures of winding were high [3]. The feedback to the operator was the frequency of the audible sound emitted by the roll during the collision with the club. The operator would hear higher frequencies in Cross Machine Direction (CMD) locations where pressures were high and lower frequencies in CMD locations where the pressures were low. This was a crude device and operator dependency could be high due to different striking methods and on the operator ability to hear the result of the strike. This spawned the development of several devices where the roll was impacted with devices that provided better control of the collision of an impactor with the roll and also qualitatively measured the dynamics of the collision.

A device that achieved good success was the Beloit Rhometer[1] [4]. This handheld instrument was rested on the surface of the wound roll and was intended to measure roll hardness. The operator pulled a trigger that raised an internal cantilever beam, with an end mass, to a set height and then quickly released the beam. The end mass, instrumented with an accelerometer, would then accelerate downward until it collided with the roll surface. At the instant of the collision deceleration would begin. The peak deceleration would be measured with the accelerometer and every 3.76 g's of deceleration would result in 1 Rho unit of output on the Rhometer display. This device could be used with much greater precision than a wooden club to seek out CMD variation in wound rolls. Collision dynamics can be greatly affected by the internal and surface properties of all bodies involved. The stiffness of the cantilever beam, the elevation which it is released, the size and shape of the end mass, the shape, stiffness and damping of the roll surface, the mass of the web layers and slip between layers during the strike will all affect the peak deceleration measured. While the Rhometer was a large step forward in the assessment of wound rolls, it suffered from an output in Rho units.

What for instance did a reading of 150 Rho taken on a roll wound of polyester film mean in comparison to a reading of 40 on the same roll at a different CMD? The roll was harder at the location where the reading of 150 Rho was taken, but what were the roll pressures at those locations? Based on the output alone there was no answer to this question, so Mollamahmutoglou et. al. [5] developed a method to attack the problem. Their method used a winding model to first determine the internal pressures for a given web under known winding conditions. The radial modulus of elasticity (E_r) for wound rolls is state dependent on the pressure exerted on a layer. After executing the winding

[1] Millassist Services Inc., 141 N. Farmer Street, Otsego, MI 49078, USA

model, the pressures due to winding were known and the radial modulus as a function of radius was also known. Then a second model was executed in the form of a dynamic contact simulation between the end mass on the cantilever beam and the surface of the wound roll. The pressures in the web layers in the contact zone beneath the end mass will further increase during the collision. The radial modulus was updated spatially as a function of these pressures during the collision. Later in the collision the dynamic pressures would decrease back to the pressures due to winding and the radial modulus would continue to update until the collision was complete. The peak deceleration of the end mass during the collision could be predicted and converted to Rho units for comparison to Rhometer test data. These simulations were difficult. It was found that slippage between web layers and the associated energy dissipation could affect the peak deceleration. To allow slippage between the web layers meant that each web layer and the contact between web layers had to be modelled. If the test and simulation decelerations were similar, the pressures and stresses output by the winding model could be deemed valid and used to assess roll defects.

BELL-2000 GEN II[1], TAPIO RQP[2] and ACA RoQ[3] are next generation instruments for measuring roll hardness. The scientific working principle is very similar to the Rhometer, but the data collection and reporting was much improved. The BELL-2000 uses a handheld modal hammer instrumented with an accelerometer and produces the Rho output units of the Rhometer. The TAPIO and ACA devices output the deceleration of a solenoid driven striker.

Another group of devices that have enjoyed success were developed by Proceq[4]. This device evolved from an instrument to test concrete hardness/strength (Schmidt Hammer) to the Parotester for testing wound rolls, to the most recent versions Equotip 550 Leeb U and PaperSchmidt. The working principle for these devices is very different than that of the Rhometer although they are similar in making a measurement involving a dynamic collision. The devices offered by Proceq make what is essentially a restitution measurement. The devices are compressed until they internally launch a mass toward a target in contact with the wound roll surface. The velocity of the mass is measured before striking and after rebounding from the target. The output of the Parotester is the rebound velocity divided by the pre-strike velocity multiplied by a 1000 and the output unit is a Paro.

The Acoustic Roll Structure Gage was invented by Swanson [6]. This method involved striking a roll from inside the core. The intent was to induce a travelling wave in the wound roll and measure the time-of-flight (*tof*) required for the wave to travel from the core to the outer surface of the wound roll. Sensors were required at the core and at the outer surface to determine the *tof*. Winding models can be used to predict roll pressures and stresses with knowledge of web and core properties, the finish radius of the roll and winding tension. A complexity of web materials wound into rolls is that the radial modulus of elasticity is not a constant. Pfeiffer [7] offered a nonlinear expression to relate pressure (P) and strain in the radial direction (ε_r):

$$P = K_1\left(e^{K_2\varepsilon_r} - 1\right) \qquad \{1\}$$

[2] Tapio Technologies Oy, Nuijalantie 13, FIN-02630 Espoo, Finland
[3] ACA Systems Oy, Outilantie 3, 83750 Sotkuma, Finland
[4] Proceq USA, Inc., 117 Corporation Drive, Aliquippa, PA 15001, USA

The parameters K_1 and K_2 were estimated by curve fitting equation {1} to pressure and strain data acquired from stacks of web in compression. The radial modulus is then:

$$E_r = \frac{dP}{d\varepsilon_r} = K_2\left(P + K_1\right) \qquad \{2\}$$

The pressure P_i in each layer i of a winding roll can be unique and is predicted using the winding model. Winding models function similar to physical winders. On a winder, the pressures change slightly throughout the roll when a new layer is added to the outside of the roll. In winding models, sets of solid mechanics equations are solved to determine the increments in pressure and stresses that resulted from the addition of the previous layer. The total pressure and stresses in a given layer are the summed result of all the increments in pressure and stresses in the given layer that resulted from winding on new layers outboard of the given layer. The radial modulus is updated within each layer as a function {2} of the total pressure in each layer. The time of flight (*tof*) of a transient pressure wave through a finished roll would be:

$$\mathrm{tof}_{\mathrm{model}} = \sum_{i=1}^{n} \frac{h_i}{\sqrt{\frac{E_{ri}(r)}{\rho_i(r)}}} \qquad \{3\}$$

where n is the number of layers, h_i, E_{ri} and ρ_i are the thickness, the radial modulus and the density of the i^{th} layer. The term under the radical is the wave velocity through the i^{th} layer. The winding tension used in the model would be iterated until the model *tof* approached the measured *tof*. Then the stresses output from the winding model, as a function of radial location, should have been those that existed within the wound roll at the CMD location where the measurement was made. This method was found not to work for all wound rolls. The difficulty was that in some cases the travelling wave would never appear at the outer surface of the wound roll such that the experimental *tof* could not be measured. The travelling wave appeared not to propagate radially to the the sensor on the outer surface of the roll. Although this method never enjoyed commercial success it was a method that resulted in knowledge of stresses within the roll that could be used to predict defects.

Roll *firmness* has been defined by a group in the paper tissue and towel sector as the amount a cylindrical stylus of fixed diameter will deform into the surface of a wound roll. The force to impart this deformation is measured and the test concludes when the measured force achieves a user defined preset value. Kershaw Instrumentation[5] markets two such devices, the RDT-2000 and the RDT-16U. The relation between load and deformation is highly nonlinear, and equation {1} demonstrates the nonlinear relation between pressure and strain in a stack has logarithmic form. These devices essentially capture one data point on the nonlinear load versus deformation curve as the stylus is impinged into the roll. The measured deformation is used as a mark of roll firmness or density in the Kershaw devices. Sartain et. al. [8] offered an alternate to the Kershaw design. A preloaded wheel is rolled across the width of a wound roll and the deformation of the wheel into the outer surface of the roll was measured. Another alternate method was to impinge the wheel at a preset deformation into the outer surface of the wound and measure the force required to maintain that deformation as the wheel rolled across the

[5] Kershaw Instrumentation LLC, 517 Auburn Avenue, Swedesboro, NJ, 08085, USA

width of the roll. This is essentially an automated embodiment of the Kershaw type measurement. The Kershaw and Sartain et. al. type measurements are quite similar to the roll hardness instruments in that an output is provided that can be used to diagnose upstream web formation or coating nonuniformity. The method falls short of predicting defects that may be witnessed when a roll is unwound.

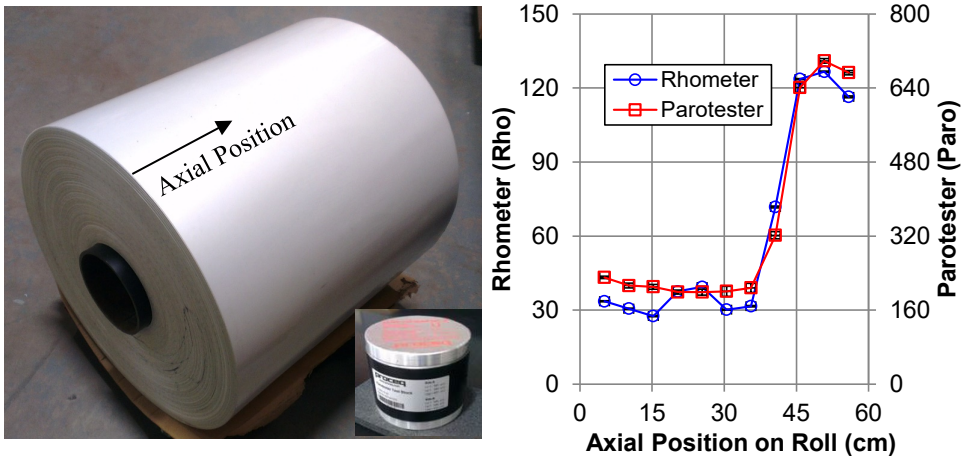

Figure 1 – Hardness Testing of a Wound Roll of Polyester Film

Regardless of whether the output units are the Rho, decelerations of a striker, the Paro or firmness, ultimately the question remains how roll quality from all perspectives is measured or inferred by a given method or device. Consider the wound roll of polyester film shown in Figure 1. Visually this appears to be a fine roll. The roll appears cylindrical and there is no telescoping. Internally there is variation in this roll, both the Rhometer and the Parotester discern appreciable hardness variation at eleven axial positions across the roll width. At each axial position five measurements were taken with each device. The mean data are shown in Figure 1 and the standard errors of the five measurements are shown as vertical error bars that are barely visible for either device. Comparison of the data from the two devices shows that both discern an increase in hardness that appears to begin at 35 cm and continue to the edge of the roll at 55 cm. Note the Rhometer also discerns an increased hardness between 15 and 30 cm that appears to have gone undetected by the Parotester.

The Parotester has a calibration standard which is essentially a cylinder with thick aluminum plates capping the cylinder ends which is also shown in Figure 1. When the Parotester is used to test the hardness of the end cap, a reading of 565 Paro units should be displayed. The Parotester unit used in this testing displayed exactly 565 Paro units on the calibration standard. The mean peak hardness of the polyester roll in Figure 1 is 699 Paro units with a standard error of 4.9 Paro units at axial position of 50.8 cm. Thus the roll of polyester film would appear “harder” than the aluminum calibration unit.

The Parotester was also used to test a roll of spunbond nonwoven web shown in Figure 2. Note the Rhometer displays 17 Rhos of hardness on the nonwoven, less than any hardness witnessed in the polyester roll. Note the Parotester displayed 739 Paro units at the same location and if truly measuring hardness the nonwoven roll would have to be judged harder than any location on the polyester film roll or the aluminum calibration

standard in Figure 1. If the output of the Parotester is treated as a restitution rather than a hardness measurement, then perhaps the output of the Parotester becomes consistent with the rebound characteristics of the two wound rolls and the calibration standard tested.

Regardless, it is apparent there is greater web thickness in the 35-55 and the 15-30 cm axial position domains that locally produced greater readings. What thickness variation exists is unknown; qualitatively it is known that there is greater thickness in those domains. There are undoubtedly higher pressures and tangential stresses in those domains but the magnitudes are unknown. Whether there is potential for inelastic deformation due to the tangential stresses is unknown. The yield strength of oriented polyester film is typically 60 MPa (8,700 psi). If the tangential stresses were known we would be able to predict if web bagginess would appear when unwinding the roll in Figure 1. Larger interlayer pressures would also be expected in these domains. If the pressures and blocking pressure was known in these domains, blocking predictions could be made. Then predictions could be made whether the roll could be unwound. Thus it is known that there is some nonuniformity in the wound roll in Figure 1 that produced some hardness variation. If the hardness variation in Figure 1 will cause loss when the web is unwound and transported through a downstream process is unknown until attempted.

Figure 2 – Hardness Testing of a Wound Roll of Nonwoven

This publication reports the development of a method that allows wound roll quality to be explored at the winder in the broadest sense to date. The method is a quantitative and scientific refinement of what the thumb can infer and can be applied to all wound rolls. There are two aspects of this study. First is determining the radial stiffness of the surface of a wound roll using a model. The second aspect is determining the radial stiffness of the outer surface of a wound roll using either commercial testing equipment or handheld instrument intentionally designed for that purpose. When the test value of the radial stiffness matches that of the model, then the internal stresses within the wound roll are known at a given CMD location. When radial stiffness tests are conducted across the roll width, then combined with the model the internal residual stresses due to winding are known spatially throughout the wound roll and defect analysis can ensue. If radial stiffness test measurements are made but not coupled with the model, these test measurements can be used similarly to a Rhometer or a Parotester to pinpoint local formation or coating non-uniformities upstream of the winder. When the test measurements are coupled with the model then defects can predicted and the wound roll

quality can be assessed that will be witnessed when the roll is unwound in the next web process line.

RADIAL ROLL SURFACE STIFFNESS TESTING

A testing device is required that will simultaneously acquire the load and the associated deformation of the roll surface as a stylus is impinged into the roll surface. Dynamic testing methods can leave indications of inelastic deformation in the roll surface. This is easily avoided in surface stiffness testing where the maximum load input to the stylus and the stylus geometry are easily controlled. In the testing done herein, the tip of the stylus was circular and 9.53 mm (3/8 inch) in diameter. Stiffness measurements can be made on smaller rolls in commercial universal testing machines such as those marketed by Instron Corporation[6] as shown in Figure 3. The logistics of testing production scale wound rolls that can be 10 m in width and 3 m in diameter in universal test machines is not feasible. When operators test production size rolls, handheld instruments that acquire the load and deformation data simultaneously and then reduce the data automatically to a radial surface stiffness are necessary. Such an instrument was developed in this study and is shown in Figure 3. It is called the Wound Roll Quality Instrument (WRQI) and was created within the Web Handling Research Center[7]. The operator selects a force range, depending on the delicacy of the surface of the wound roll, and begins making measurements by pressing the stylus into the surface of the roll The instrument continually records the load and deformation of the stylus until the upper force range is reached. The calculated stiffness, in engineering units, is then displayed on the meter's screen.

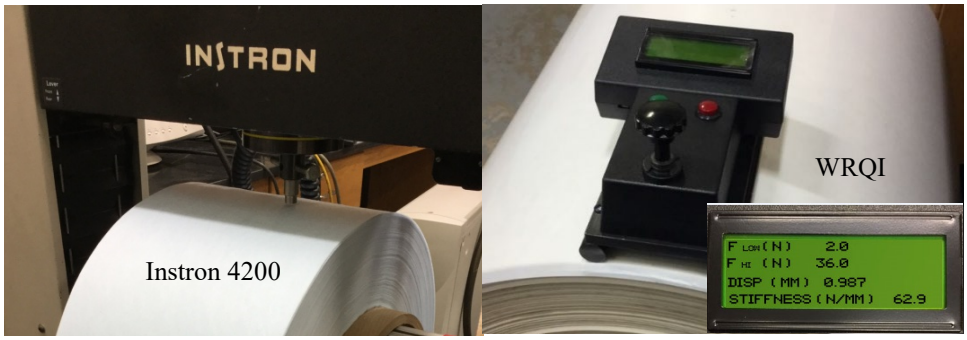

Figure 3 – Surface Stiffness Testing Instruments: Instron 4200 and WRQI

THE WRQI MODEL FOR PREDICTING RADIAL SURFACE STIFFNESS

Models have existed for some time that allow the internal residual stresses in a roll due to winding to be found as a function of web and core properties and winder operating conditions such as winding tension. Increased winding tension will commensurately increase the radial stiffness of the outer surface of a wound roll. Increasing winding tension will also produce increased pressures as a function of radius P(r) in the wound roll. The increase in pressure will produce an increase in radial modulus E_r {2}

[6] Instron, 825 University Ave, Norwood, MA, 02062-2643 USA
[7] Web Handling Research Center, Oklahoma State University, Stillwater, OK, USA

throughout a roll. The increase in radial modulus is responsible for increasing the radial stiffness of the wound roll. To predict the radial stiffness requires two sub models. The first sub model will predict how the radial modulus varies through the radius of the winding roll. The second sub model is a contact model between the finished wound roll surface and a stylus. This model will apply successive larger contact loads on the stylus that will cause the stylus to deform the surface of the wound roll. With known contact loads and accompanying deformations the radial stiffness of the outside of the wound roll can be determined.

The Wound Roll Sub Model

The first portion of the model is based on an axisymmetric one-dimensional finite element formulation that is used to model the internal residual stresses and deformations due to winding. The axis of symmetry here is the z axis, the axial direction in the wound roll shown in Figure 4. The formulation predicts the changes in radial deformations and stresses as each layer is added to the winding roll. These changes in radial deformations and stresses are used to update the total deformations, the total radial locations of all layers and the total stresses in each layer throughout the winding roll. In Figure 4 a natural coordinate ξ is assumed in a master element that can range from -1 to 1 in the r-direction from nodes *i* to *j*. Shape functions are assumed for this 1D finite element model development which allow linear variation in a given variable:

$$N_i = \frac{1-\xi}{2} \quad N_j = \frac{1+\xi}{2} \qquad \{4\}$$

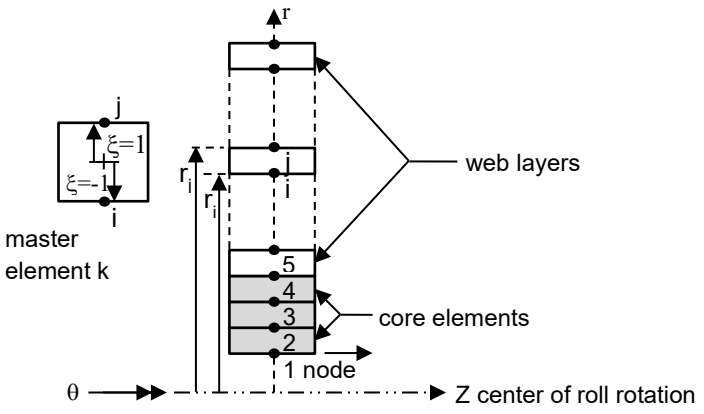

Figure 4 – 1D Axisymmetric Finite Element Model of Wound Roll

The radial displacement of any point within the domain of an element is given by:

$$u = \begin{bmatrix} N_i & N_j \end{bmatrix} \begin{Bmatrix} u_i \\ u_j \end{Bmatrix} \qquad \{5\}$$

where u_i and u_j are the deformations of nodes i and j in the radial direction in Figure 4. An isoparametric formulation is assumed, thus a radial location within an element can also be interpolated using the shape functions:

$$r = \begin{bmatrix} N_i & N_j \end{bmatrix} \begin{Bmatrix} r_i \\ r_j \end{Bmatrix} \quad \{6\}$$

The coordinate map between the r and ξ coordinate systems is:

$$\xi = \frac{2}{r_j - r_i}\left(r - \frac{r_i + r_j}{2}\right) \quad \{7\}$$

The strain terms are needed to form the strain energy and the element stiffness matrix. The radial strain ε_r is developed using the simplification that $r_j - r_i$ is the deformable web thickness h:

$$\varepsilon_r = \frac{du}{dr} = \frac{du}{d\xi}\frac{d\xi}{dr} = \begin{bmatrix} -\frac{1}{h} & \frac{1}{h} \end{bmatrix} \begin{Bmatrix} u_i \\ u_j \end{Bmatrix} \quad \{8\}$$

The tangential strain is calculated at the centroid $\bar{r} = \frac{r_i + r_j}{2}$ of the element:

$$\varepsilon_\theta = \frac{u}{r} = \begin{bmatrix} \frac{N_i}{r} & \frac{N_j}{r} \end{bmatrix} \begin{Bmatrix} u_i \\ u_j \end{Bmatrix} = \begin{bmatrix} \frac{1}{2\bar{r}} & \frac{1}{2\bar{r}} \end{bmatrix} \begin{Bmatrix} u_i \\ u_j \end{Bmatrix} \quad \{9\}$$

The strains related to the z-direction are taken as zero due to the assumption of plane strain:

$$\varepsilon_z = \gamma_{rz} = 0 \quad \{10\}$$

The nonzero strains can be written:

$$\begin{Bmatrix} \varepsilon_r \\ \varepsilon_\theta \end{Bmatrix} = \begin{bmatrix} -\frac{1}{h} & \frac{1}{h} \\ \frac{1}{2\bar{r}} & \frac{1}{2\bar{r}} \end{bmatrix} \begin{Bmatrix} u_i \\ u_j \end{Bmatrix} = \begin{bmatrix} \bar{B} \end{bmatrix} \{u\} \quad \{11\}$$

The constitutive relations are needed to relate strains to stresses. Note Maxwell's relations were employed to enforce symmetry ($\frac{\nu_{\theta r}}{E_\theta} = \frac{\nu_{r\theta}}{E_r}$ $\frac{\nu_{zr}}{E_z} = \frac{\nu_{rz}}{E_r}$ $\frac{\nu_{z\theta}}{E_z} = \frac{\nu_{\theta z}}{E_\theta}$). Also note that $\nu_{\theta r}$ and ν_{zr} were selected, rather than $\nu_{r\theta}$ and ν_{rz}, for input as they will be physically larger and easier to measure for typical cases where E_r is much smaller than E_θ and E_z:

$$\begin{Bmatrix}\varepsilon_r\\ \varepsilon_\theta\\ \varepsilon_z\end{Bmatrix}=\begin{bmatrix}\frac{1}{E_r} & -\frac{\nu_{\theta r}}{E_\theta} & -\frac{\nu_{zr}}{E_z}\\ -\frac{\nu_{\theta r}}{E_\theta} & \frac{1}{E_\theta} & -\frac{\nu_{z\theta}}{E_z}\\ -\frac{\nu_{zr}}{E_z} & -\frac{\nu_{z\theta}}{E_z} & \frac{1}{E_z}\end{bmatrix}\begin{Bmatrix}\sigma_r\\ \sigma_\theta\\ \sigma_z\end{Bmatrix} \quad \{12\}$$

The assumption of plain strain allows the 3rd row in {10} to be modified:

$$\varepsilon_z = 0 = -\frac{\nu_{zr}}{E_z}\sigma_r - \frac{\nu_{z\theta}}{E_z}\sigma_\theta + \frac{\sigma_z}{E_z} \quad or \quad \sigma_z = \nu_{zr}\sigma_r + \nu_{z\theta}\sigma_\theta \quad \{13\}$$

The modified constitutive matrix can be written:

$$\{\varepsilon\}=\begin{Bmatrix}\varepsilon_r\\ \varepsilon_\theta\end{Bmatrix}=\begin{bmatrix}\frac{1}{E_r}-\frac{\nu_{zr}^2}{E_z} & -\frac{\nu_{\theta r}}{E_\theta}-\frac{\nu_{zr}\nu_{z\theta}}{E_z}\\ -\frac{\nu_{\theta r}}{E_\theta}-\frac{\nu_{zr}\nu_{z\theta}}{E_z} & \frac{1}{E_\theta}-\frac{\nu_{z\theta}^2}{E_z}\end{bmatrix}\begin{Bmatrix}\sigma_r\\ \sigma_\theta\end{Bmatrix}=[D]^{-1}\{\sigma\} \quad \{14\}$$

Inversion provides the [D] matrix:

$$[D]=\frac{E_\theta\begin{bmatrix}E_r\left(E_\theta\nu_{z\theta}^2-E_z\right) & -E_r\left(E_\theta\nu_{zr}\nu_{z\theta}+E_z\nu_{\theta r}\right)\\ -E_r\left(E_\theta\nu_{zr}\nu_{z\theta}+E_z\nu_{\theta r}\right) & E_\theta\left(E_r\nu_{zr}^2-E_z\right)\end{bmatrix}}{E_z\left(E_r\nu_{\theta r}^2-E_\theta\right)+E_\theta\left(E_\theta\nu_{z\theta}^2+E_r\nu_{zr}\left(\nu_{zr}+2\nu_{z\theta}\nu_{\theta r}\right)\right)}=\begin{bmatrix}D_{11} & D_{12}\\ D_{21} & D_{22}\end{bmatrix} \quad \{15\}$$

The D matrix will be unique for the core and web since the modulus and Poisson ratio terms will be unique. The D matrix will be unique for each web layer *i* due to the known state dependency of the radial modulus of a web E_{ri} on the pressure P_i on that layer {2}. The *D* matrix must be positive definite for stable finite element computations that do not violate physical reality. If the following conditionals are satisfied the D matrix will be positive definite:

$$\begin{gathered}E_r,\ E_\theta,\ E_z > 0\\ |\nu_{\theta r}| < \sqrt{\frac{E_\theta}{E_r}} \quad |\nu_{zr}| < \sqrt{\frac{E_z}{E_r}} \quad |\nu_{z\theta}| < \sqrt{\frac{E_z}{E_\theta}}\\ 1-\nu_{r\theta}\nu_{\theta r}-\nu_{\theta z}\nu_{z\theta}-\nu_{zr}\nu_{rz}-2\nu_{\theta r}\nu_{z\theta}\nu_{rz} > 0\end{gathered} \quad \{16\}$$

In rare cases the *D* matrix may be found not to be positive definite after measuring the web properties. In those cases the *D* matrix is unknown.

Given the D matrix the stress and strain can be related using:

$$\{\sigma\}=[D]\{\varepsilon\}=[D]\left[\overline{B}\right]\{u\} \quad \{17\}$$

The displacements of all the layers are calculated when a new incoming web is added. The incoming web layer has initial strain ε_o due to initial stresses σ_o resulting from web tension.

The total potential energy Π_e for the element is composed of strain energy and work potential terms:

$$\Pi_e = \frac{1}{2}\int_0^{2\pi}\int_A \{\sigma\}^T \{\varepsilon\} r \; dA \; d\theta - \int_0^{2\pi}\int_A \{\sigma\}^T \{\varepsilon_o\} r \; dA \; d\theta \qquad \{18\}$$

and after substitution of {10} and {15}:

$$\Pi_e = \frac{2\pi}{2}\{u\}^T \int_A \{\bar{B}\}^T [D]\{\bar{B}\}\bar{r} \; dA\{u\} - 2\pi\{u\}^T \int_A \{\bar{B}\}^T [D]\{\varepsilon_o\}\bar{r} \; dA \qquad \{19\}$$

Through collection of terms equation {20} can be restated in terms of a stiffness matrix and force vector for each element:

$$\Pi_e = \frac{1}{2}\{u\}^T [K_e]\{u\} - \{u\}^T \{f_e\} \qquad \{20\}$$

where:

$$[K_e] = 2\pi\int_A \{\bar{B}\}^T [D]\{\bar{B}\}\bar{r} \; dA = 2\pi\bar{r}A_e \{\bar{B}\}^T [D]\{\bar{B}\} = 2\pi\bar{r}hW \{\bar{B}\}^T [D]\{\bar{B}\} \qquad \{21\}$$

$$\{f_e\} = 2\pi\int_A \{\bar{B}\}^T [D]\{\varepsilon_o\}\bar{r} \; dA = 2\pi\bar{r}hW \{\bar{B}\}^T [D]\{\varepsilon_o\} = 2\pi\bar{r}hW \{\bar{B}\}^T \{\sigma_o\} \qquad \{22\}$$

where W is the web width. After substitution of $\bar{B}$ and D:

$$[K_e] = \begin{bmatrix} \frac{\pi W}{2}\left(\frac{4\bar{r}}{h}D_{11} + \frac{h}{\bar{r}}D_{22} - 4D_{12}\right) & \pi W\left(\frac{h}{2\bar{r}}D_{22} - \frac{2\bar{r}}{h}D_{11}\right) \\ \pi W\left(\frac{h}{2\bar{r}}D_{22} - \frac{2\bar{r}}{h}D_{11}\right) & \frac{\pi W}{2}\left(\frac{4\bar{r}}{h}D_{11} + \frac{h}{\bar{r}}D_{22} + 4D_{12}\right) \end{bmatrix} = \begin{bmatrix} k_{11} & k_{12} \\ k_{21} & k_{22} \end{bmatrix} \qquad \{23\}$$

$$\{f_e\} = 2\pi\bar{r}hW \begin{Bmatrix} \frac{\sigma_\theta}{2\bar{r}} - \frac{\sigma_r}{h} \\ \frac{\sigma_\theta}{2\bar{r}} + \frac{\sigma_r}{h} \end{Bmatrix}_0 \qquad \{24\}$$

The only non-zero pre-stress σ_o in a new element of web added to the outside of a winding roll is the stress due to web tension ($\sigma_o = \sigma_\theta = T_w$). There were no radial stress terms in the incoming web prior to contact of the winding roll. Hence the elemental for vector simplifies to:

$$\{f_e\} = -\pi hWT_w \begin{Bmatrix} 1 \\ 1 \end{Bmatrix} \qquad \{25\}$$

Note that a minus sign appears in {25} that was not present in {24}. This was introduced to account for the direction of loads in Figure 4. A positive web tensile stress T_w in the tangential θ direction will produce negative u deformations in Figure 4.

Now that the stiffness and load formulations for an element are complete, global assembly equations are formed composed of core elements and the web layer elements up to the most recent layer wound on the outside of the roll. An example is shown for the assembled equations {24} for the case where a third web layer has just been wound on the outside of a winding roll. The core is modelled using two axisymmetric finite elements to reduce the size of the matrix which is typically insufficient to model the stresses through the thickness of the core correctly, five elements are usually sufficient. The orthotropic material {14} and stiffness {21} developments can be uniquely applied to the core elements and web layers. The c subscripts in {24} denote stiffness terms from core elements and the w subscripts denote stiffness terms related to web layers. The three web layers are modelled with one axisymmetric finite element each which is sufficient to well model the membrane strains and stresses:

$$\begin{bmatrix} k_{11\boxed{c1}} & k_{12\boxed{c1}} & 0 & 0 & 0 & 0 \\ k_{12\boxed{c1}} & k_{22\boxed{c1}} + k_{11\boxed{c2}} & k_{12\boxed{c2}} & 0 & 0 & 0 \\ 0 & k_{12\boxed{c2}} & k_{22\boxed{c2}} + k_{11\boxed{w1}} & k_{12\boxed{w1}} & 0 & 0 \\ 0 & 0 & k_{12\boxed{w1}} & k_{22\boxed{w1}} + k_{11\boxed{w2}} & k_{12\boxed{w2}} & 0 \\ 0 & 0 & 0 & k_{12\boxed{w2}} & k_{22\boxed{w2}} + k_{11\boxed{w3}} & k_{12\boxed{w3}} \\ 0 & 0 & 0 & 0 & k_{12\boxed{w3}} & k_{22\boxed{w3}} \end{bmatrix} \begin{Bmatrix} \delta u_1 \\ \delta u_2 \\ \delta u_3 \\ \delta u_4 \\ \delta u_5 \\ \delta u_6 \end{Bmatrix} = \begin{Bmatrix} 0 \\ 0 \\ 0 \\ 0 \\ -\pi h_w W T_w \\ -\pi h_w W T_w \end{Bmatrix} \quad \{26\}$$

This system of equations is now solved for all nodal deformations δu_j throughout the core and web layers due to the addition of the third layer. As each new layer is added to the outside of the winding roll all the nodes will deform uniquely δu_i inward in small increments. This system of equations is reformed and resolved for the addition of every layer wound onto the roll. After each solution the incremental deformations can be used to update the total deformation of a given web layer and the deformed radial locations of all web layers. These deformations are calculated for all the nodes for the addition of the n^{th} layer and are used to update the total deformation of all nodes:

$$u_i = \sum_{j=1}^{\text{core elements}+n+1} \delta u_{i,j} \quad \{27\}$$

$$r_i = r_i + u_i \quad \{28\}$$

Some means must be used to determine when the addition of layers will cease based on user choice. One scenario could be to cease adding web layers whenever the radial location of the outermost node exceeds a user designated finish radius r_{fin} for the wound roll. Another scenario might be to cease adding layers when a user designated number of layers n have been wound onto the core. The centroidal r locations of all layers can be determined, for the k$^{\text{th}}$ layer:

$$\overline{r_k} = \frac{r_i + r_j}{2} \quad \{29\}$$

where the i^{th} and j^{th} nodes bound the k^{th} layer. After a layer has been wound onto the roll the changes in deformations of all nodes $\{\delta u\}$ are known through solution of equations such as those shown in equation {25}. These increments in deformation cause increments

in stress which can be determined in each layer using equations {13} and {17}. For the k^{th} layer bounded by the i^{th} and j^{th} nodes:

$$\begin{Bmatrix} \delta\sigma_r \\ \delta\sigma_\theta \end{Bmatrix}_k = [D]_k \begin{Bmatrix} \delta\varepsilon_r \\ \delta\varepsilon_\theta \end{Bmatrix}_k = [D]_k \left[\overline{B}\right]_k \begin{Bmatrix} \delta u_i \\ \delta u_j \end{Bmatrix} \qquad \{30\}$$
$$\delta\sigma_{zk} = \nu_{zr}\delta\sigma_{rk} + \nu_{z\theta}\delta\sigma_{\theta k}$$

In equation {30} recognize the D matrix is unique in layer k as the radial modulus E_{rk} is dependent on the total pressure in that layer P_k (P_k=-σ_{rk}). The total stresses in the k^{th} layer are the $\delta\sigma$ stresses when the k^{th} layer was added to the roll plus all the increments in $\delta\sigma$ stresses in the k^{th} layer due to layers that were added after the k^{th} layer. If the roll currently has n layers wound onto the core, the stress in the k^{th} layer will be:

$$\{\sigma\}_k = \begin{Bmatrix} \sum_{i=k}^{n} \delta\sigma_{ri,k} \\ \sum_{i=k}^{n} \delta\sigma_{\theta i,k} + T_w \\ \sum_{i=k}^{n} \delta\sigma_{zi,k} \end{Bmatrix} = \begin{Bmatrix} \sigma_r \\ \sigma_\theta \\ \sigma_z \end{Bmatrix}_k \qquad \{31\}$$

The D matrix would now be updated for the n layers that have been wound onto the roll as a function of the total pressure P_k (P_k=-σ_{rk}) in each of the layers and use of equation {2} The stress state for the current outer layer (layer 3 in equation {26}) cannot be determined using equation {30} since the radial deformations of the current outer layer are unknown at that instant in the calculations. The pressure in the outer layer (P) is estimated using equilibrium:

$$P = \frac{T_w h}{s} \qquad \{32\}$$

where s was the outer radius of the wound roll when the previous layer was added and predicted using equation {28}. The radial modulus of the outer layer can then be determined using equation {2}. Now the solution process can continue with the addition of another web layer. When the roll has finished winding the final stress levels are known in every layer and the radial modulus is known in every web layer.

The Contact Sub Model

The completion of the execution of the winding sub model is the starting point for execution of the contact sub model. The contact sub model does not involve the accretion of layers, the roll has been completely wound in the winding sub model. The contact sub model is also a nonlinear axisymmetric finite element model but now the axis of symmetry has become the radial direction of the wound roll and is now concentric with the axis of the cylindrical stylus used to make the stiffness measurements. The stylus is 9.53 mm (0.375 in) in diameter and assumed rigid in comparison to the web layers that will be contacted. The winding sub model was a simplified one dimensional finite element formulation in the radial direction; hence the only non-zero deformations were the u deformations of equation {5}. In the contact sub model two dimensional axisymmetric deformations (u, w) were needed in the (r, z) directions as shown in

Figure 5. The assumption of axisymmetric deformation about the axis of the stylus is reasonable and greatly reduces the size of the sets of equation that must be solved. Quadrilateral finite elements were used as shown in Figure 5 and each quadrilateral sweeps 2π radians about the z axis.

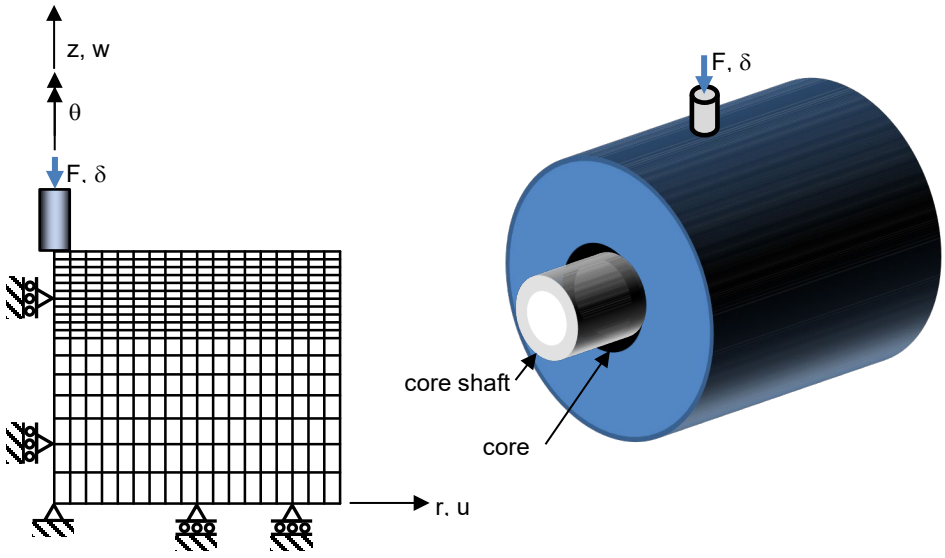

Figure 5 – 2D Axisymmetric Finite Element Contact Model of Stylus with Wound Roll

The 2D deformation (u, w) field was needed in the contact sub model to capture the state of deformation surrounding the stylus as the contact load F is increased from F_{low} to F_{high}. There will be significant shearing strain and stress in the surface of the wound roll due to the impingement of the stylus into the wound roll. Thus the constitutive relations have increased in complexity from equation {14} as a result of including shearing strain and not enforcing the plane strain condition assumed in the winding model.

$$\begin{Bmatrix} \varepsilon_{r-con} \\ \varepsilon_{z-con} \\ \gamma_{rz-con} \\ \varepsilon_{\theta-con} \end{Bmatrix} = \begin{Bmatrix} \frac{\partial u}{\partial r} \\ \frac{\partial w}{\partial z} \\ \frac{\partial u}{\partial z} + \frac{\partial w}{\partial r} \\ \frac{u}{r} \end{Bmatrix} = \begin{bmatrix} \frac{1}{E_{r-con}} & -\frac{\nu_{zr}}{E_{z-con}} & 0 & -\frac{\nu_{\theta r}}{E_{\theta-con}} \\ -\frac{\nu_{rz}}{E_{r-con}} & \frac{1}{E_{z-con}} & 0 & -\frac{\nu_{\theta z}}{E_{\theta-con}} \\ 0 & 0 & \frac{1}{G_{rz-con}} & 0 \\ -\frac{\nu_{r\theta}}{E_{r-con}} & -\frac{\nu_{z\theta}}{E_{z-con}} & 0 & \frac{1}{E_{\theta-con}} \end{bmatrix} \begin{Bmatrix} \sigma_{r-con} \\ \sigma_{z-con} \\ \tau_{rz-con} \\ \sigma_{\theta-con} \end{Bmatrix} \quad \{33\}$$

Here $E_{z\text{-}con}$ is state dependent on $\sigma_{z\text{-}con}$ stress level and is defined using equation {2}. $E_{\theta\text{-}con}$ is the modulus of the web in the machine direction and $E_{r\text{-}con}$ is the modulus of the web in the cross machine direction. In the winding sub model the height of each element is taken as the thickness of the web h. The initial values of $E_{z\text{-}con}$ would be the average radial modulus of all layers whose radius falls within the z domain of a given finite element in the contact sub model. Axisymmetric quadrilateral finite elements with orthotropic

material behaviors are common and will not be presented here. The contact sub model increases the applied force on the stylus from a low preset level F_{low} to a high level F_{high} in increments. These levels of load will also be employed by the device that is used in the test assessment of the surface stiffness of the roll. After each increment of load is added the average σ_z stress level is assessed within each finite element. The modulus of each element in the z direction ($E_{z\text{-}con}$) is then updated per equation {2} prior to the application of the next increment of load.

At each load level within the domain [F_{low}, F_{high}] the load level F and the stylus deformation δ into the surface of the wound roll is saved. After computations have completed at all load levels, the nonlinear relationship between the contact force F and corresponding surface deformation δ is known and the average contact stiffness of the wound roll for the given stylus geometry can be assessed. In Figure 5 a core and a supporting core shaft that may or may not be present are shown. It is assumed for the cases that will be demonstrated here that the stiffness of the core and the core shaft are large relative to the stiffness of the surface of the wound roll where the stiffness measurement is made. Based on this assumption the rigid roller constraints preventing w deformations were enforced. This is not a limitation of the method, the stiffness of the core and a core shaft when present can be included in the contact model.

The derivation of the quadrilateral finite element model is not provided here. There are many commercial finite element codes that have axisymmetric quadrilateral elements with orthotropic elastic material behavior [9]. Many codes as well have nonlinear solution methods in place to model inelastic material behavior that will allow the modulus $E_{z\text{-}con}$ to vary as a function of a strain or stress level in an element ($\varepsilon_{z\text{-}con}$ or $\sigma_{z\text{-}con}$) using an equation {2} or a lookup table.

APPLICATION OF THE WRQI MODEL

The model will be applied for two unique webs. One web was a Melinex 377 polyester biaxial oriented web provided by Dupont Teijin Films[8]. This film has high surface roughness (2.12 μm) which causes the radial modulus (E_r) to be small compared to the MD modulus (E_θ). For a polyester web, Melinex 377 has high radial compressibility. The second web is very different from the PET web. It is a Spunbond-Meltblown-Spunbond (SMS) nonwoven web (22 gsm) developed by Kimberly-Clark Corporation[9]. In comparison to the polyester web the nonwoven is very extensible in the MD direction and very compressible in the radial direction. This comparison will be noted in the modulus properties of the two webs presented in Table 1. Each web will be wound at four winding tensions.

After the winding sub model has executed the residual stresses due to winding are known. With known internal pressure as a function of radius the radial modulus after winding is also known as shown in Figure 6. The radial modulus after winding has finished will be needed by the contact sub model to compute the stiffness of the roll surface. The tangential and axial stresses are now known and shown in Figures 7 and 8.

The contact sub-model begins execution directly after the winding sub-model completes. The contact model performs calculations for stiffness over the load range [F_{low},F_{high}] which were identified in Table 1. The WRQI can make measurements in several user defined load ranges. In Table 1 it should be noted that F_{low} was set at 2.22 N

[8] Dupont Teijin Films, 3600 Discovery Drive, Chester, VA 23836, USA
[9] Kimberly-Clark Corporation, 351 Phelps Drive Irving, Texas 75038, USA

while F_{high} was set at 40 N for the Melinex 377 web whereas it was set at 13.3 N for the SMS nonwoven web. The SMS web is relatively delicate in comparison to the Melinex 377 polyester web. The WRQI is intended to be a non-destructive test. The value of F_{high} should be set to ensure no permanent deformation is visible on the roll surface after testing.

model			web	
winding	contact		Melinex 377	SMS
h			50.8 μm (0.002 in)	88.9 μm (0.0035 in)
E_θ	$E_{\theta\text{-con}}$		4.90 GPa (711,000 psi)	104 MPa (15,061 psi)
E_z	$E_{r\text{-con}}$		4.90 GPa (711,000 psi)	104 MPa (15,061 psi)
E_r	$E_{z\text{-con}}$	K_1	22.0 KPa (3.19 psi)	3.55 KPa (0.515 psi)
		K_2	38.6	7.525
$\nu_{\theta r}$, ν_{zr}, $\nu_{z\theta}$			0.3	0.3
E_c			207 GPa (30E06 psi)	3.45 GPa (500,000 psi)
ν_c			0.3	0.3
$r_{core\ inner}$			3.81 cm (1.5 in)	8.57 cm (3.375 in)
r_{core}			4.29 cm (1.688 in)	9.84 cm (3.875 in)
r_{finish}			11.91 cm (4.688 in)	17.8 cm (7 in)
T_w winding tensions			2.24 MPa (325 psi)	197 KPa (28.6 psi)
			4.48 MPa (650 psi)	393 KPa (57.1 psi)
			6.72 MPa (975 pli)	591 KPa (85.7 psi)
			8.96 MPa (1300 psi)	788 KPa (114.3 psi)
F_{low}			2.22 N (0.5 lb)	2.22 N (0.5 lb)
F_{high}			40 N (9 lb)	13.3 N (3 lb)

Table 1 – Web and Core Properties and Winding Tensions

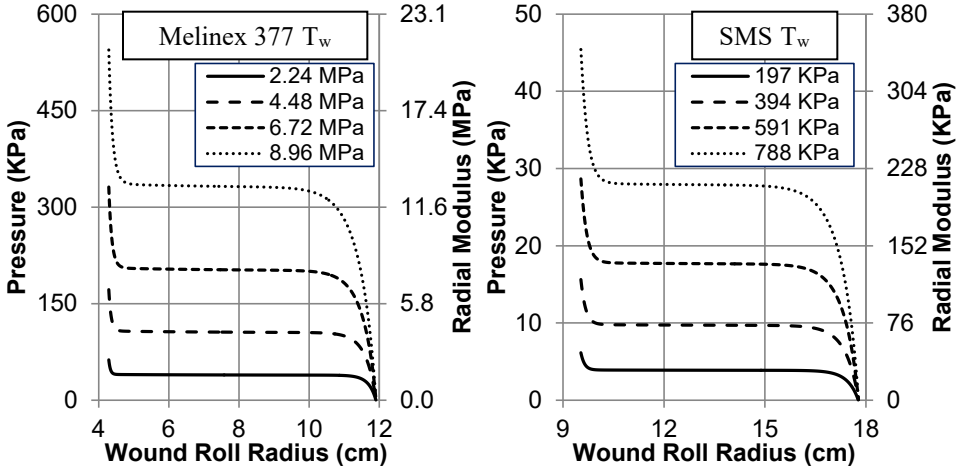

Figure 6 – Residual Pressure and Radial Modulus after winding for the Melinex 377 and SMS webs.

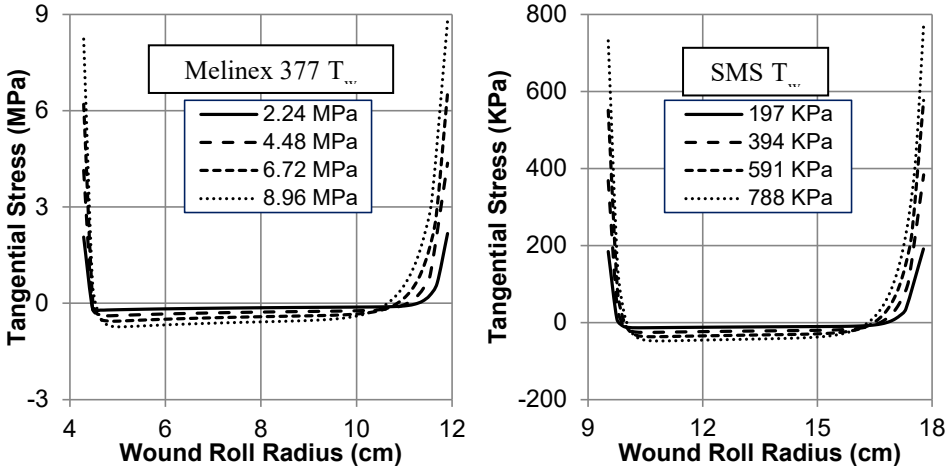

Figure 7 – Tangent Stresses after Winding the Melinex 377 and SMS webs.

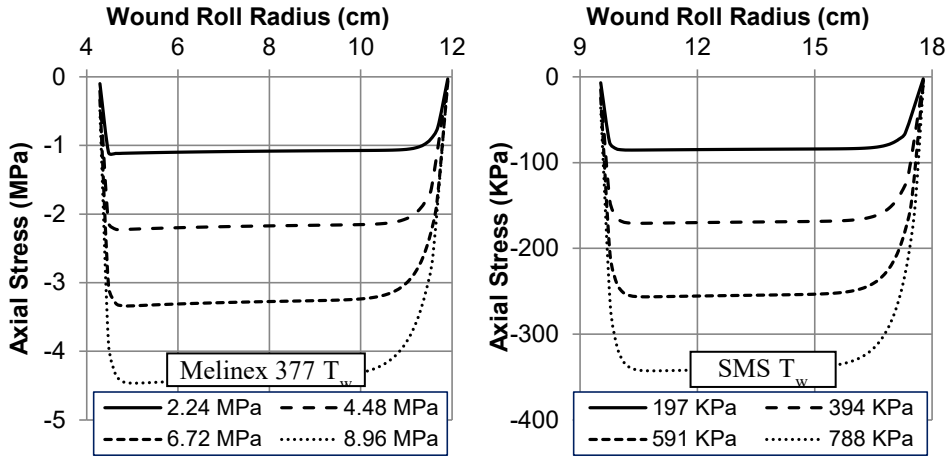

Figure 8 – Axial Stresses after Winding the Melinex 377 and SMS webs.

In Figures 9 and 10 the stylus contact load versus surface deformation are shown for the two web materials. Here the test data was provided by the Instron 4200 commercial material testing system. The stylus tip is small enough that the contact area between the tip and the wound roll is the entirety of the tip area over the test load range. The nonlinearity between load and deformation in Figures 9 and 10 is due to the state dependent modulus $E_{z\text{-}con}$ which increases in the finite elements beneath the stylus as the pressures between the layers increase with test load. The Instron tests were repeated three times for each winding tension, the repeatability for all winding tensions is very good. The agreement between the WRQI model result and the Instron test data is quite good for all winding tension cases for the Melinex 377 web in Figure 9. For the SMS nonwoven

web results in Figure 10, the agreement is quite good at the higher winding tensions but there is some disagreement which is worst for the lowest winding tension.

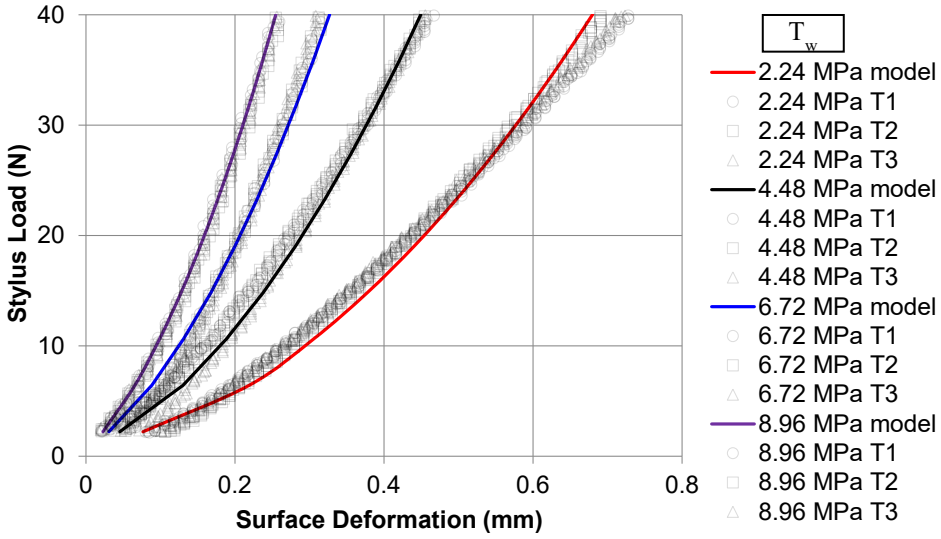

Figure 9 – Model and Instron Test load/Deformation for Melinex 377 rolls.

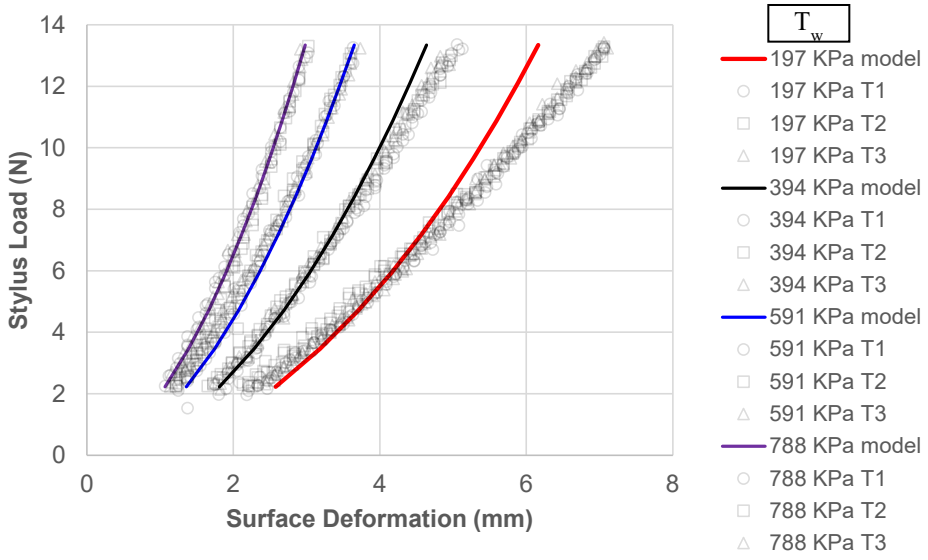

Figure 10 – Model and Instron Test load/Deformation for SMS nonwoven rolls.

In Figures 9 and 10 the nonlinearity of the surface stiffness with respect to load or surface deformation can be noted. The WRQI produces an average measurement of the surface stiffness over the range of stylus force [F_{low}, F_{high}]. Tabular comparisons comparing stiffness results made with WRQI, the Instron 4200 and the model are

presented for the SMS nonwoven and Melinex 377 rolls in Tables 2 and 3, respectively. These results show good comparison between the WRQI and Instron measurements as well as good comparisons of measurements and the model results. The benefit of the modeling is that in predicting the radial stiffness the winding residual stresses presented in Figures 6, 7 and 8 are now known and can be used to predict winding defects.

Winding Tension (KPa)	Stiffness (N/mm)		
	Meter	Instron	Model
197	3.01	2.33	3.12
394	3.50	3.45	3.96
591	4.38	4.54	4.89
788	5.50	5.90	5.87

Table 2 – Stiffness for SMS rolls

Winding Tension (MPa)	Stiffness (N/mm)		
	Meter	Instron	Model
2.24	64.7	60.1	64.4
4.48	94.1	88.3	95.6
6.72	136.6	146.1	129.8
8.96	173.7	163.8	165.2

Table 3 – Stiffness for Melinex 377 rolls

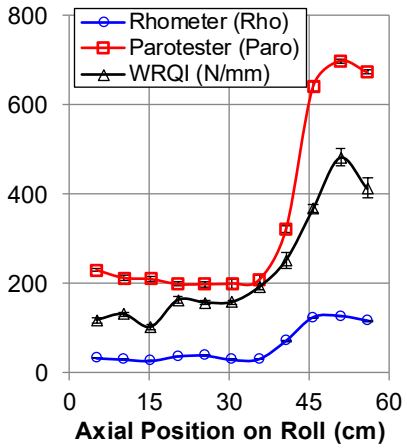

Figure 11 – Testing of the Polyester Roll from Figure 1

The WRQI can be used in a standalone fashion for studying CMD variation due to web or coating thickness variation. This is demonstrated in Figure 11 on the polyester roll that was presented in Figure 1. Note that all devices capture the gross left to right variation. The small decline witnessed at 15 cm by the Rhometer and the WRQI was not detected by the Parotester. The decrease at the right edge was witnessed more clearly by the Parotester and the WRQI than by the Rhometer. One should not expect to shift the results presented in Figure 11 using a constant factor due to nonlinearities involved in the measurements.

The contact sub model developed herein is much simpler than the dynamic collision model that Mollamahmutoglou et. al. [5] developed to study the contact of the Rhometer with a wound roll. The contact sub model is easily coupled to 2D axisymmetric wound roll models [10, 11] such that the residual stresses due to winding (e.g. Figures 6-8) can be explored over the roll width.

CONCLUSIONS

A new method for investigating wound roll quality has been developed. The novelty of the development is that much deeper investigation of wound roll quality is now possible. Previous measurement devices have fallen short from coupling the measurement acquired to the conditions inside the wound roll that produced the measurement. It is the winding residual stress conditions that are largely responsible for producing the winding defects that dictate the quality of a wound roll. Thus, it is appropriate the method and device be named the Wound Roll Quality Instrument/ Method, it is the first of its kind.

ACKNOWLEDGEMENTS

The authors would like to thank the sponsors of the Web Handling Research Center at Oklahoma State University for supporting the research that made this development possible. Oklahoma State University has patents pending on the technologies described herein.

REFERENCES

1. Bufton, M. J., Marklin, R.W., Nagurka, M. L., and Simoneau, G. G., "Effect of Keyswitch Design of Desktop and Notebook Keyboards Related to Key Stiffness and Typing Force," Ergonomics, Vol. 49, No. 10, 2006, pp. 996-1012.
2. Abbott, J. A., "Quality Measurement of Fruits and Vegetables," Postharvest Biology and Technology, Vol. 15, 1999, pp. 207-225.
3. Good, J. K. and Roisum, D. R., Winding: Machines, Mechanics and Measurements, TAPPI Press, pp. 301-303.
4. Good, J. K. and Roisum, D. R., Winding: Machines, Mechanics and Measurements, TAPPI Press, pp. 303-306.
5. Mollamahmutoglu, C., Bulut, O., Adari, S. and Good, J. K., "The Coupling of Winding Models and Roll Quality Instruments," The 13th International Conference on Web Handling, Oklahoma State University, Stillwater, OK, 2015.
6. Swanson, R. P., "Determination of Wound Roll Structure using Acoustic Time of Flight Measurement," The 1st International Conference on Web Handling, Oklahoma State University, Stillwater, OK, 1991, pp. 57-67.
7. Pfeiffer, J. D., "Internal Pressures in a Wound Roll of Paper," TAPPI Journal, Vol. 49, No. 8, 1966, pp. 342-347.
8. Sartain, K., Harris, N., Wojcik, S., Urquhart, R., Daniels, M. and Baggot, J., "Roll Firmness Measuring System and Process," US Patent Application Publication: US 2007/0012119 A1.
9. Chandrupatla, T. R., and Belegundu, A. D., Introduction to Finite Elements in Engineering, 4th edition, Pearson, 2012.
10. Good, J. K., Mollamahmutoglu, C., Markum, R. and Gale, J. W., "Residual Winding Stresses Due to Spatial Web Thickness Variation," ASME Journal of Manufacturing Science and Engineering, Vol. 139, No. 3, March 2017.
11. Mollamahmutoglu, C., and Good, J. K., "Modeling the Influence of Web Thickness and Length Imperfections Resulting from Manufacturing Processes on Wound Roll Stresses," CIRP Journal of Manufacturing Science and Technology, Vol. 8, January 2015, pp. 22-33.